Journal of Drug Delivery Science and Technology 114 (2025) 107520

Contents lists available at ScienceDirect

Journal of Drug Delivery Science and Technology

journal homepage: www.elsevier.com/locate/jddst

Dual-crosslinked injectable *in situ* forming Alginate/$CaCl_2$/Pluronic F127/α-Cyclodextrin hydrogels incorporating Doxorubicin and graphene-based nanomaterials for cancer chemo-photothermal therapy

Joaquim J. Gonçalves [a,b], Bruna L. Melo [a,b], Manuel R. Pouso [a], Ilídio J. Correia [a,b,c,*], Duarte de Melo-Diogo [a,**]

[a] RISE-Health – Departamento de Ciências Médicas, Faculdade de Ciências da Saúde, Universidade da Beira Interior, Av. Infante D. Henrique, 6200-506, Covilhã, Portugal
[b] AEROG-LAETA, Aerospace Sciences Department, Universidade da Beira Interior, Covilhã, Portugal
[c] University of Coimbra, CERES, Department of Chemical Engineering, 3030-790, Coimbra, Portugal

ARTICLE INFO

Keywords:
Cancer
Chemo-photothermal therapy
Graphene family nanomaterials
Injectable hydrogels
Local delivery
Macroscale delivery systems

ABSTRACT

Injectable *in situ* forming hydrogels have been emerging due to their capacity to perform the direct delivery of therapeutics into the tumor site with minimal off-target leakage. Particularly, physical crosslinked injectable *in situ* forming hydrogels are appealing due to their straightforward preparation that exploits the native jointing capabilities of specific polymers/materials. However, the features of these hydrogels (*e.g.*, injectability, degradation, swelling) are strongly pre-determined by the physical interactions available on the selected polymers/materials, occasionally yielding undesired outcomes. Thus, the combination of multiple physical crosslinking cues may allow the preparation of hydrogels with enhanced properties. In this work, a dual-crosslinked injectable *in situ* forming hydrogel was engineered by combining Pluronic F127/α-Cyclodextrin and Alginate/$CaCl_2$ (*i.e.*, combination of host-guest and electrostatic interactions), being loaded with Doxorubicin (chemotherapeutic drug) and Dopamine-reduced Graphene Oxide (photothermal nano-agent) for application in cancer chemo-photothermal therapy. When compared to the single-crosslinked hydrogels, the dual-crosslinking contributed to the assembly of formulations with suitable injectability and improved degradation and water absorption behaviors. Moreover, the dual-crosslinked hydrogels presented a good photothermal capacity ($\Delta T \approx 14$ °C), leading to a 1.18-times enhanced Doxorubicin release. In *in vitro* cell-based studies, the dual-crosslinked hydrogels exhibited an excellent cytocompatibility towards healthy (normal human dermal fibroblasts) and breast cancer (MCF-7) cells. As importantly, the dual-crosslinked hydrogels were able to mediate a chemo-photothermal effect that diminished the cancer cells' viability to just 23 %. Overall, the developed dual-crosslinked injectable *in situ* forming hydrogels incorporating Doxorubicin and Dopamine-reduced Graphene Oxide are a promising macroscale system for breast cancer chemo-photothermal therapy.

1. Introduction

In the last decade, a boom in the development of nanomaterials for anticancer applications has occurred [1–3]. Such rise was triggered by the nanostructures propensity to reach the tumor zone through the *so-called* Enhanced Permeability and Retention (EPR) effect. In brief, the tumor zone has an aberrant leaky vasculature (with fenestrae of 200–1200 nm) and a defective lymphatic drainage [4,5]. Thus, by taking advantage of the EPR effect, nanostructures with well-tailored physicochemical properties (*e.g.*, size, surface charge, corona composition) can accumulate and become stationed at the tumor site [4,6,7]. Some nanostructures can further capitalize on this effect by enrolling on combinatorial therapeutic approaches, opening a venue for more effective cancer treatments [8–10].

Among the different combinatorial approaches, the synergy between nanomaterials' photothermal therapy and chemotherapy has been yielding very exciting results [11–13]. In this combinatorial modality,

* Corresponding author. AEROG-LAETA, Aerospace Sciences Department, Universidade da Beira Interior, Covilhã, Portugal.
** Corresponding author. RISE-Health – Departamento de Ciências Médicas, Faculdade de Ciências da Saúde, Universidade da Beira Interior, Av. Infante D. Henrique, 6200-506, Covilhã, Portugal.)
E-mail addresses: icorreia@ubi.pt (I.J. Correia), demelodiogo@fcsaude.ubi.pt (D. de Melo-Diogo).

https://doi.org/10.1016/j.jddst.2025.107520
Received 9 April 2025; Received in revised form 8 September 2025; Accepted 9 September 2025
Available online 11 September 2025

Abbreviations:

ANOVA Analysis of variance
Calcium Chloride $CaCl_2$
DLS Dynamic light scattering
DMEM-F12 Dulbecco's modified Eagle's medium F-12
DOPA-rGO Dopamine-reduced graphene oxide
DOPA-rGO@A_{Ca}Gel DOPA-rGO loaded Alginate/$CaCl_2$ hydrogel
DOPA-rGO@P_{CD}Gel DOPA-rGO loaded Pluronic F127/α-Cyclodextrin hydrogel
DOPA-rGO@$P_{CD}A_{Ca}$Gel DOPA-rGO loaded Pluronic F127/α-Cyclodextrin/Alginate/$CaCl_2$ hydrogel
DOX Doxorubicin
DOX + DOPA-rGO@$P_{CD}A_{Ca}$Gel DOX and DOPA-rGO loaded Pluronic F127/α-Cyclodextrin/Alginate/$CaCl_2$ hydrogel
EPR Enhanced permeability and retention
FBS Fetal bovine serum
FTIR Fourier-transform infrared
MCF-7 Michigan cancer foundation-7
NHDF Normal human dermal fibroblasts
NIR Near infrared
NS Non-significant
PBS Phosphate buffered saline
PI Propidium iodide
S.D Standard Deviation
SEM Scanning Electron Microscopy
TEM Transmission Electron Microscopy
W/NIR With NIR laser exposure
W/o NIR Without NIR laser exposure

drug-loaded nanomaterials with light-absorbing capabilities are systemically administered [14,15]. Once the nanomaterials reach the tumor site, this zone is irradiated with light, and the nanostructures convert the absorbed light into heat (photothermal therapy) [14,15]. The nanostructures' photothermal heating can *per se* induce damages on cancer cells, leading in some cases to their death [16]. These hyperthermic effects can also trigger the release of the loaded drug or can sensitize cancer cells to chemotherapeutics' action, leading to a synergistic therapeutic outcome [17,18].

From the myriad of nanomaterials with potential to be applied in cancer chemo-photothermal therapy, those based on Dopamine-reduced Graphene Oxide (DOPA-rGO) have been receiving a great interest. Such is correlated with the capacity of DOPA-rGO to absorb near-infrared (NIR; 750–1000 nm) light and with its large surface area [19]. Due to its high NIR absorption, the DOPA-rGO can generate a temperature increase upon interaction with NIR light [19]. This capacity is of paramount importance since the NIR light *per se* has a good penetration depth and it displays minimal interactions with biological components (*e.g.*, water, hemoglobin, melanin) [20]. In this way, the photoinduced heat prompted by DOPA-rGO can achieve a good spatio-temporal resolution with diminished off-target interactions [19]. On the other hand, the large surface area of DOPA-rGO is compatible with the loading of several bioactive drugs [21,22], allowing their delivery to cancer cells. As importantly, the DOPA-rGO nanomaterials have a straightforward preparation and are highly cytocompatible [19].

Despite the potential of the nanomaterials aimed for cancer chemo-photothermal therapy, their translation into the clinic has not yet been achieved. In fact, an exhaustive literature analysis has revealed that less than 1 % (median) of the nanostructures administered systemically accumulate at the tumor site [23]. In one hand, the nanostructures can suffer opsonization once in the bloodstream, leading to their rapid clearance [24,25]. On the other hand, systemically administered nanomaterials have been engineered to achieve tumor accumulation based on the principles of the EPR effect [26,27]. However, the EPR effect is not universally present in all human solid tumors, being, in fact, overexaggerated on pre-clinical cancer models [26,28].

To address this issue, researchers have just started to explore the potential of injectable *in situ* forming hydrogels for executing the direct delivery of light-responsive nanomaterials/drugs into the tumor (local administration) [17,29]. In this technological approach, an aqueous solution containing the hydrogel precursor materials (*e.g.*, polymers, crosslinkers) and the therapeutic compounds (*e.g.*, NIR-light responsive nanomaterials, chemotherapeutic drugs) is loaded into a syringe, being injected intratumorally [17]. Subsequently, the hydrogel suffers *in situ* gelation through physical and/or chemical crosslinking, performing a tumor-confined delivery of the therapeutics with minimal off-target leakage [17]. Chemical crosslinking strategies based on Photopolymerization and Thiol-Maleimide, Schiff-base or Tetrazine-Norbornene reactions have been explored to mediate the *in situ* assembly of injectable hydrogels [30–35]. These covalent reactions can offer a precise control of the hydrogels' properties but require the chemical modification of the polymers with compatible functional groups (a laborious and complex procedure) and may demand specific reaction conditions (*e.g.*, photoinitiators, pH) [30–36]. In turn, physical crosslinked hydrogels can be prepared using readily available and affordable polymers/materials by exploiting their native jointing capabilities (*e.g.*, through Host-Guest or Electrostatic interactions) [37,38]. Still, the properties of these hydrogels (*e.g.*, injectability, gelation time, degradation, swelling) are strongly pre-determined by the physical interactions available on the selected polymers/materials, occasionally yielding undesired outcomes [39–41]. For instance, the reversible nature of the Host-Guest interactions established between α-Cyclodextrin (host) and Pluronic F127 (guest) facilitates the preparation of hydrogels with a good injectability [41]. However, the reversible character of these Host-Guest interactions can also cause the premature collapse of the Pluronic F127/α-Cyclodextrin hydrogels when in contact with biological fluids [40]. The combination of Alginate (negatively charged) and $CaCl_2$ (provides positively charged Calcium ions (Ca^{2+})) can also mediate the fast *in situ* gelation of injectable hydrogels through electrostatic interactions [39]. However, a dense electrostatic crosslinking degree can yield hydrogels with a high rigidity/low flexibility, which may not mediate a uniform delivery of the loaded therapeutics along the tumor mass [39]. In this way, the combination of multiple physical crosslinking cues may allow the preparation of injectable *in situ* forming hydrogels with enhanced properties.

So far, single-physical crosslinked injectable *in situ* forming hydrogels assembled using Chitosan/$NaHCO_3$ (electrostatic interactions) have been developed to encapsulate DOPA-rGO and Resveratrol for use in cancer chemo-photothermal therapy [42]. Dual-physical crosslinked injectable *in situ* forming hydrogels produced by combining Pluronic F127 and Chitosan/$NaHCO_3$ (hydrophobic and electrostatic interactions) were also engineered to load DOPA-rGO for application in cancer photothermal therapy [43]. However, to the best of our knowledge, multiple-physical crosslinked injectable *in situ* forming hydrogels co-encapsulating DOPA-rGO nanomaterials and chemotherapeutic drugs aimed for cancer chemo-photothermal therapy have not yet been explored.

In this work, a dual-physical crosslinked injectable *in situ* forming hydrogel incorporating Doxorubicin (DOX) and DOPA-rGO was prepared, for the first time, for application in cancer chemo-photothermal therapy. The dual-physical crosslinked injectable hydrogel was engineered by combining Pluronic F127/α-Cyclodextrin (host-guest interaction) and Alginate/$CaCl_2$ (electrostatic interaction). After the hydrogel's assembly, its physicochemical and biological properties were

characterized.

2. Materials and methods

2.1. Materials

Pluronic F127, α-Cyclodextrin, DOX, Graphene oxide, Sodium alginate, Dulbecco's Modified Eagle's Medium F12 (DMEM F-12), Penicillin/Streptomycin, Resazurin, Trypsin and Phosphate Buffered Saline Solution (PBS) were obtained from Sigma-Aldrich (Sintra, Portugal). Dopamine hydrochloride was obtained from Acros Organic (New Jersey, USA). Fetal Bovine Serum (FBS) was acquired from Biochrom AG (Berlin, Germany). Calcium chloride ($CaCl_2$) and Propidium Iodide (PI) were purchased from Alfa Aesar (Massachusetts, USA). Calcein-AM was obtained from Merck Milipore (Algés, Portugal). Michigan Cancer Foundation-7 (MCF-7) cell line was provided by ATCC (Middlesex, UK). Normal Human Dermal Fibroblasts were purchased from PromoCell (Heidelberg, Germany). T-flasks and cell culture plates were acquired from Thermo Fisher Scientific (Porto, Portugal). CellTiter-Glo® 2.0 was acquired from Promega (Wisconsin, USA). Double-deionized and filtered water (0.22 μm filtered; 18.2 MΩ cm) was used in this work.

2.2. Methods

2.2.1. Synthesis and characterization of DOPA-rGO

Dopamine-reduced graphene oxide (DOPA-rGO) was synthesized using the method previously described by Lima-Sousa and colleagues [19]. Prior to the synthesis, graphene oxide was sonicated for 6 h. Afterwards, the graphene oxide solution (5 mL; 500 μg/mL) was mixed with Dopamine hydrochloride (12.5 mg) and NaOH (10 mM; to achieve a pH 8.5), being left to react under stirring at 60 °C for 4 h. Then, the resulting material was purified via dialysis against water for 2 h (14 KDa molecular weight cut-off membrane), yielding DOPA-rGO.

To characterize the DOPA-rGO, Dynamic Light Scattering Analysis (DLS) was employed to analyze its nanometric size distribution (Zetasizer Nano ZS, Malvern Instruments, Worcestershire, UK) [21]. The DOPA-rGO size and morphology were also visualized through Transmission Electron Microscopy (TEM; Hitachi-HT7700, Tokyo, Japan; accelerating voltage of 80 kV). Before this analysis, the DOPA-rGO was stained with phosphotungstic acid (2 % (w/v)) [21]. By last, absorption spectroscopy was used to verify the NIR absorption of DOPA-rGO (Evolution 201 spectrophotometer, Thermo Scientific., Massachusetts, USA) [19].

2.2.2. Formulation of the dual-crosslinked injectable in situ forming hydrogels

The production of the dual-crosslinked injectable *in situ* forming hydrogel incorporating DOX and DOPA-rGO (designated as DOX + DOPA-rGO@$P_{CD}A_{Ca}$Gel) was performed by employing a Pluronic F127:α-Cyclodextrin mass ratio of 6.51:9.72 (to coordinate the host-guest interactions) and Alginate:$CaCl_2$ mass ratio of 4:1 (to coordinate the electrostatic interactions) [39,44]. To do so, initially a solution composed of Pluronic F127 (350 mg/mL) and $CaCl_2$ (53.8 mg/mL) was prepared and kept in an ice-cold bath. Parallelly, a solution containing Alginate (22.1 mg/mL), α-Cyclodextrin (53.6 mg/mL), DOPA-rGO and DOX was prepared. Afterwards, the Pluronic F127/$CaCl_2$ (18.6 μL) and the Alginate/α-Cyclodextrin/DOPA-rGO/DOX (181.4 μL) solutions were mixed, loaded into a syringe equipped with a 21G needle (0.8 × 40 mm) and extruded, leading to the assembly of the DOX + DOPA-rGO@$P_{CD}A_{Ca}$Gel (28.25 μg of DOPA-rGO; 12.2 μg of DOX). The Pluronic F127/$CaCl_2$ (18.6 μL) and the Alginate/α-Cyclodextrin/DOPA-rGO/DOX (181.4 μL) solutions were also extruded into microtubes, being the assembled hydrogels recovered in order to obtain formulations with constant macroscopic dimensions. A dual-crosslinked injectable *in situ* forming hydrogel incorporating only DOPA-rGO (termed as DOPA-rGO@$P_{CD}A_{Ca}$Gel) was also prepared as described above but without the DOX addition step.

As controls, single-crosslinked hydrogels incorporating DOPA-rGO were also prepared. In this regard, hydrogels composed of Pluronic F127, α-Cyclodextrin, and DOPA-rGO were also produced (designated as DOPA-rGO@P_{CD}Gel). For such, the Pluronic F127:α-Cyclodextrin mass ratio and the DOPA-rGO content were kept unchanged but the total DOPA-rGO@P_{CD}Gel weight was adjusted to match that of DOPA-rGO@$P_{CD}A_{Ca}$Gel. With the same purpose, hydrogels formed with Alginate, $CaCl_2$ and DOPA-rGO were also created (designated as DOPA-rGO@A_{Ca}Gel). Similarly, the Alginate:$CaCl_2$ mass ratio and the DOPA-rGO content were kept unchanged but the total DOPA-rGO@A_{Ca}Gel weight was adjusted to match that of DOPA-rGO@$P_{CD}A_{Ca}$Gel.

2.2.3. Characterization of the physicochemical properties of the hydrogels

The injectability and *in situ* gelation of the DOX + DOPA-rGO@$P_{CD}A_{Ca}$Gel, DOPA-rGO@$P_{CD}A_{Ca}$Gel, DOPA-rGO@P_{CD}Gel, and DOPA-rGO@A_{Ca}Gel were assessed by extruding their corresponding precursor mixtures through syringes fitted with 21G needles (0.8 × 40 mm) [42]. The gelation of these formulations was also confirmed through the inverted microtube test [42]. To accomplish that, the hydrogels' precursor solutions were loaded into microtubes, being these placed at room temperature and then inverted. The cross-section morphology of DOX + DOPA-rGO@$P_{CD}A_{Ca}$Gel and DOPA-rGO@$P_{CD}A_{Ca}$Gel was assessed by Scanning Electron Microscopy (SEM) [45]. For such, these samples were placed on aluminum stubs and sputter-coated with gold (Quorum Q150R ES sputter coating device, Quorum Technologies Ltd., Laughton, East Sussex, UK). Subsequently, the SEM images were acquired by utilizing a Hitachi S-3400N Scanning Electron Microscope (Hitachi, Tokyo, Japan). The chemical composition of the DOX + DOPA-rGO@$P_{CD}A_{Ca}$Gel and DOPA-rGO@$P_{CD}A_{Ca}$Gel was determined by Fourier-transform infrared (FTIR) spectroscopy (Nicolet iS10 spectrometer, Thermo Scientific Inc., Massachusetts, USA). To determine the DOX encapsulation efficiency in the DOX + DOPA-rGO@$P_{CD}A_{Ca}$Gel, this formulation was first removed from the microtubes. Afterwards, the hydrogel-free microtubes were washed with methanol to recover the non-encapsulated DOX. Then, the non-loaded DOX content was determined by fluorescence spectroscopy ($\lambda_{Excitation}$ = 488 nm, $\lambda_{Emission}$ = 590 nm; FluoroMax-4 spectrofluorometer, Horiba, Kyoto, Japan).

The Gel fraction of DOX + DOPA-rGO@$P_{CD}A_{Ca}$Gel and DOPA-rGO@$P_{CD}A_{Ca}$Gel was determined by adapting a previously reported protocol [46]. In brief, the hydrogel formulations were submerged in water at 37 °C, under shaking. After 1 h, the hydrogels were recovered, freeze-dried (ScanVac CoolSafe, LaboGene ApS, Lynge, Denmark), and weighed. The Gel fraction was calculated according to Eq. (1) (W_i is the initial weight of the hydrogels; W_1 is the weight of the hydrogels after 1 h of incubation).

$$Gel\ fraction\ (\%) = \frac{W_1}{W_i} \times 100\ \% \quad \text{(Eq. 1)}$$

The degradation profile of the different hydrogels was assessed as previously defined elsewhere [45]. To do so, the DOX + DOPA-rGO@$P_{CD}A_{Ca}$Gel, DOPA-rGO@$P_{CD}A_{Ca}$Gel, DOPA-rGO@P_{CD}Gel, and DOPA-rGO@A_{Ca}Gel were submerged in PBS (pH 7.4) at 37 °C, under shaking, for 7 days. At specific pre-determined timepoints, the hydrogels were extracted, washed with water, freeze-dried, and subsequently weighed. The weight loss was calculated, at each designated timepoint, using Eq. (2) (W_i is the initial weight of the hydrogels; W_t is the weight of the hydrogels at time t).

$$Weight\ loss\ (\%) = \frac{W_i - W_t}{W_i} \times 100\ \% \quad \text{(Eq. 2)}$$

The water absorption capacity of the hydrogels (correlates to the swelling) was determined following a formerly established protocol [45]. In brief, the DOX + DOPA-rGO@$P_{CD}A_{Ca}$Gel, DOPA-rGO@$P_{CD}A_{Ca}$Gel, DOPA-rGO@P_{CD}Gel, and DOPA-rGO@A_{Ca}Gel were submerged in PBS (pH 7.4) at 37 °C, under shaking. At each specific

timepoint, the hydrogels were extracted from the PBS solution and then weighed. The formula used to evaluate the water absorption capacity, at each designated timepoint, is given by Eq. (3) (W_t is the weight of the hydrogels at time t; W_i is the initial weight of the hydrogel).

$$\textit{Water absorption capacity}\ (\%) = \frac{w_t - w_i}{W_i} \times 100\ \% \qquad \text{(Eq. 3)}$$

The photothermal heating generated by DOX + DOPA-rGO@$P_{CD}A_{Ca}$Gel, DOPA-rGO@$P_{CD}A_{Ca}$Gel and $P_{CD}A_{Ca}$Gel was investigated by applying a protocol previously outlined by our team [42]. For such, the hydrogels were immersed in water and posteriorly, these were irradiated with NIR light (808 nm, 1.7 W/cm^2) for 10 min. A thermocouple thermometer was then employed to monitor the temperature changes. As a control, the temperature variation of water exposed to NIR light was also assessed. To determine the release profile of DOX from DOX + DOPA-rGO@$P_{CD}A_{Ca}$Gel, this formulation was immersed in a PBS solution (pH 7.4) at 37 °C, under shaking. At pre-determined timepoints, the DOX released was measured by analyzing the DOX fluorescence ($\lambda_{Excitation}$ = 488 nm, $\lambda_{Emission}$ = 590 nm; SpectraMax Gemini EM spectrofluorometer, Molecular Devices LLC, California, USA) [47]. The influence of NIR light on DOX release was also investigated by irradiating the DOX + DOPA-rGO@$P_{CD}A_{Ca}$Gel at the 2-h timepoint (808 nm, 1.7 W/cm^2, 10 min).

2.2.4. Assessment of the DOPA-rGO@$P_{CD}A_{Ca}$Gel cytocompatibility

To assess the cytocompatibility of DOPA-rGO@$P_{CD}A_{Ca}$Gel, this formulation was placed in contact with NHDF (healthy cell model) and MCF-7 cells (breast cancer cell model), being the cells' viability determined using the resazurin assay [47]. Both cell lines were cultured in DMEM F-12 medium supplemented with 10 % (v/v) of FBS and 1 % (v/v) penicillin/streptomycin in an humified incubator (5 % CO_2, 37 °C).

To execute this assay, the cells were seeded at a density of 2.5 x 10^4 cells/well into 24-well plates. After 48 h of their seeding, the cells were incubated with fresh culture medium along with DOPA-rGO@$P_{CD}A_{Ca}$Gel for 24 and 48 h. After that, the DOPA-rGO@$P_{CD}A_{Ca}$Gel was removed, being the cells incubated with fresh medium containing resazurin (10 % (v/v)) for 4 h in the dark (5 % CO_2, 37 °C). Finally, the cellular viability was evaluated by measuring the fluorescence of resorufin ($\lambda_{Excitation}$ = 560 nm, $\lambda_{Emission}$ = 590 nm; SpectraMax Gemini EM spectrofluorometer, Molecular Devices LLC, California, USA). Cells only incubated with medium (*i.e.*, without hydrogels) were used as the negative control (K^-). Alternatively, cells incubated with ethanol (70 % (v/v)) were employed as the positive control (K^+).

2.2.5. Evaluation of the photothermal therapy mediated by DOPA-rGO@$P_{CD}A_{Ca}$Gel and chemo-photothermal therapy mediated by DOX + DOPA-rGO@$P_{CD}A_{Ca}$Gel

The photothermal therapy mediated by DOPA-rGO@$P_{CD}A_{Ca}$Gel and chemo-photothermal therapy mediated by DOX + DOPA-rGO@$P_{CD}A_{Ca}$Gel were assessed through the resazurin method as our group earlier described [47]. For this purpose, the MCF-7 cells were seeded as mentioned in section 2.2.4. After 48 h of their seeding, the MCF-7 cells were incubated with fresh culture medium along with DOPA-rGO@$P_{CD}A_{Ca}$Gel (DOPA-rGO: 56.5 μg/mL) and DOX + DOPA-rGO@$P_{CD}A_{Ca}$Gel (DOPA-rGO: 56.5 μg/mL; DOX: 24.4 μg/mL). After 2 h of incubation, the hydrogels were irradiated with NIR light (808 nm, 1.7 W/cm^2, 10 min). After totaling 24 h of incubation with the hydrogels, the MCF-7 cells' viability was determined using the resazurin method following the protocol described in section 2.2.4. The hydrogels' phototherapeutic capacity was also confirmed using the CellTiter-Glo® 2.0 assay (ATP-based cell viability determination), following the manufacturer's protocol. Additionally, Calcein-AM (labels live cells) and PI (labels dead cells) staining was also performed on the MCF-7 cells, being the imaging experiments conducted in a Zeiss Axio Observer Z1 (Carl Zeiss AG, Oberkochen, Germany) equipped with Filter Set 20 and 38 HE.

2.2.6. Statistical analysis

Comparison between multiple groups was conducted via one-way Analysis of Variance (ANOVA), with the Student-Newman-Keuls test. Comparison between two groups was conducted by the unpaired *t*-test. Results were considered statistically significant if the *p*-value was lower than 0.05 ($p < 0.05$). Analysis of the data was performed using GraphPad Prism v6.0 (Trial version, GraphPad Software, CA, USA).

3. Results and discussion

3.1. Formulation and characterization of DOX + DOPA-rGO@$P_{CD}A_{Ca}$Gel and DOPA-rGO@$P_{CD}A_{Ca}$Gel

For engineering a dual-crosslinked injectable hydrogel aimed for cancer chemo-photothermal therapy, DOX (chemotherapeutic agent) and DOPA-rGO (photothermal nanoagent) were incorporated into hydrogels assembled by combining Pluronic F127/α-Cyclodextrin (host-guest interaction) and Alginate/$CaCl_2$ (electrostatic interaction) - designated as DOX + DOPA-rGO@$P_{CD}A_{Ca}$Gel (Fig. 1A). Similarly, a dual-crosslinked injectable hydrogel designed for cancer photothermal therapy was also prepared by loading DOPA-rGO into the hydrogels assembled with Pluronic F127/α-Cyclodextrin and Alginate/$CaCl_2$ - designated as DOPA-rGO@$P_{CD}A_{Ca}$Gel. The nanometric size distribution of DOPA-rGO was confirmed by DLS and TEM (Fig. S1A and S1B). As importantly, the size of DOPA-rGO felt within the range considered to be optimal for cancer-related applications (100–200 nm) – Fig. S1C. The TEM data also showed that DOPA-rGO has the sheet-like morphology characteristic of the graphene-based nanomaterials (Fig. S1B) [21]. Absorption spectroscopy also confirmed the high NIR absorption of DOPA-rGO, a crucial feature for its use as a photothermal agent (Fig. S1D). As control, injectable hydrogels with a single crosslinking chemistry (*i.e.*, host-guest or electrostatic) were also prepared. Thus, hydrogels composed of Pluronic F127, α-Cyclodextrin, and DOPA-rGO were also produced (designated as DOPA-rGO@P_{CD}Gel). With the same purpose, hydrogels formed with Alginate, $CaCl_2$ and DOPA-rGO were also created (designated as DOPA-rGO@A_{Ca}Gel).

Initially, the injectability and *in situ* gelation of the different hydrogels were investigated. By loading the precursor solutions of DOX + DOPA-rGO@$P_{CD}A_{Ca}$Gel and DOPA-rGO@$P_{CD}A_{Ca}$Gel into a syringe, these could be extruded and achieved gelation *in situ* (Fig. 1B and C). The gelation of the DOX + DOPA-rGO@$P_{CD}A_{Ca}$Gel and DOPA-rGO@$P_{CD}A_{Ca}$Gel was also confirmed through the inverted microtube test (Fig. S2A and S2B). The injectability and *in situ* gelation of the DOX + DOPA-rGO@$P_{CD}A_{Ca}$Gel and DOPA-rGO@$P_{CD}A_{Ca}$Gel is a feature fundamental for their direct administration at the tumor zone, potentially allowing the delivery of the therapeutic agents (*i.e.*, DOX and DOPA-rGO) into the target site with minimal off-target leakage [17]. Similarly, the DOPA-rGO@P_{CD}Gel precursor solutions also demonstrated injectability and capacity to gelate *in situ* (Figs. S3A and S2C). Even though the DOPA-rGO@A_{Ca}Gel precursor solution could form a hydrogel (Fig. S2D), this formulation could not be injected since it rapidly clogged the injection apparatus (Fig. S3B). The faster gelation of DOPA-rGO@A_{Ca}Gel and its apparent greater rigidity may have contributed to its non-injectability.

Subsequently, the precursor solutions of the different hydrogels were also deposited on microtubes and then recovered (Fig. S4). Such enabled the production of hydrogels with equal macroscopic dimensions for the following studies (Fig. S4). Further assessment highlighted that DOX + DOPA-rGO@$P_{CD}A_{Ca}$Gel, DOPA-rGO@$P_{CD}A_{Ca}$Gel and DOPA-rGO@P_{CD}Gel had a uniform distribution of the therapeutic agents (Fig. S4A–S4C). In contrast, DOPA-rGO@A_{Ca}Gel could not homogenously disperse the DOPA-rGO (Fig. S4D). The irregular incorporation of the DOPA-rGO in DOPA-rGO@A_{Ca}Gel is likely correlated with the quick gelation of this formulation, potentially impacting its capacity to efficiently sustain the delivery of the loaded therapeutics. In fact, Chao et al. demonstrated that Alginate hydrogels crosslinked with Ca^{2+} (electrostatic interactions) displaying a high Alginate content do not mediate a

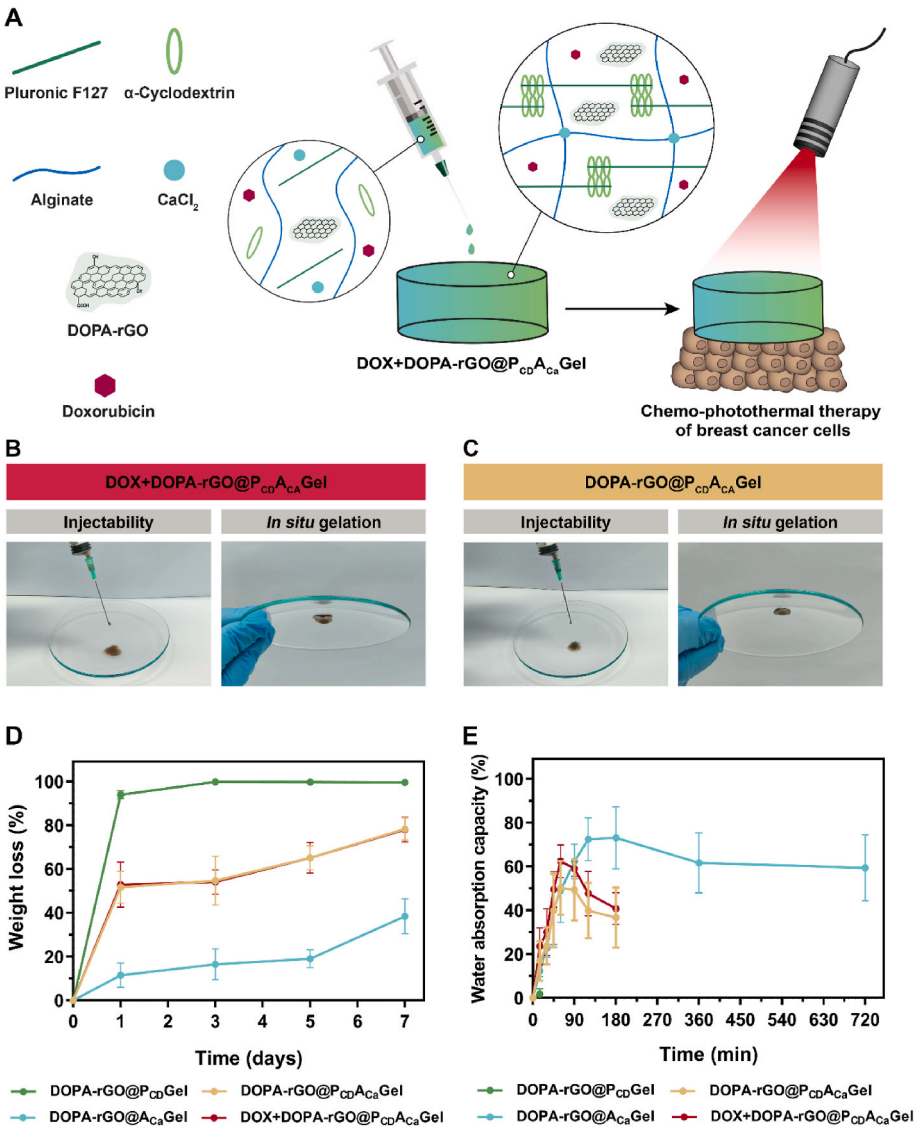

Fig. 1. Physicochemical characterization of DOX + DOPA-rGO@$P_{CD}A_{Ca}$Gel and DOPA-rGO@$P_{CD}A_{Ca}$Gel. (A) Schematic representation of the formulation of DOX + DOPA-rGO@$P_{CD}A_{Ca}$Gel and its application in the chemo-photothermal therapy of breast cancer cells. Injectability and *in situ* gelation of (B) DOX + DOPA-rGO@$P_{CD}A_{Ca}$Gel and (C) DOPA-rGO@$P_{CD}A_{Ca}$Gel. (D) Evaluation of the hydrogels' weight loss over a period of 7 days. Data represents mean ± S.D., n = 5. (E) Characterization of the hydrogels' water absorption capacity during 720 min. Data represents mean ± S.D., n = 5.

uniform delivery of the loaded therapeutics [39]. Afterwards, the Gel fraction of DOX + DOPA-rGO@$P_{CD}A_{Ca}$Gel and DOPA-rGO@$P_{CD}A_{Ca}$Gel was determined (Fig. S5). As expected, both formulations revealed a similar Gel fraction of about 66–69 % (n = 3; Fig. S5). The chemical composition of the DOX + DOPA-rGO@$P_{CD}A_{Ca}$Gel and DOPA-rGO@$P_{CD}A_{Ca}$Gel was also confirmed by FTIR (Fig. S6), further corroborating the successful preparation of the dual-crosslinked hydrogels.

Afterwards, the degradation profile of the developed hydrogels was assessed in biologically mimicking conditions (Fig. 1D). The DOX + DOPA-rGO@$P_{CD}A_{Ca}$Gel and DOPA-rGO@$P_{CD}A_{Ca}$Gel exhibited a similar degradation profile. After 1 day, these formulations lost about 52 % of their weight. In the subsequent days, the DOX + DOPA-rGO@$P_{CD}A_{Ca}$Gel and DOPA-rGO@$P_{CD}A_{Ca}$Gel continued to gradually lose their mass, achieving a 78 % degradation after 7 days (Fig. 1D). Such degradation was also visualized by SEM, which highlighted that the inner structure of the dual-crosslinked hydrogels gradually changed over time (Fig. S7). Hence, the degradation behavior exhibited by DOX + DOPA-rGO@$P_{CD}A_{Ca}$Gel and DOPA-rGO@$P_{CD}A_{Ca}$Gel may enable a sustained release of the loaded therapeutic agents. As importantly, such degradation behavior is also crucial to avoid the long-term residence of the hydrogels after their administration. In stark contrast, DOPA-rGO@P_{CD}Gel became almost completely degraded in just 3 h (weight loss ≈ 85 %; Fig. S8), demonstrating a poor stability in biologically mimicking conditions. Furthermore, the degradation profile of DOPA-rGO@P_{CD}Gel could lead to a premature and uncontrolled release of the therapeutics, compromising the hydrogels' anticancer activity. In fact, Pradal et al. has described the quick collapse of hydrogels assembled using only Pluronic F127 and α-Cyclodextrin (host-guest interaction) [40]. A similar behavior has also been reported for other Pluronic F127-based hydrogels [43]. On the contrary, the DOPA-rGO@A_{Ca}Gel demonstrated a very slow degradability, only achieving 11 and 38 % weight loss after 1 and 7 days, respectively (Fig. 1D). Such behavior implies that DOPA-rGO@A_{Ca}Gel would display a slow body clearance, which is not ideal since it could introduce unwanted effects. For instance, Su et al. also observed that Alginate hydrogels crosslinked with Ca^{2+} (electrostatic interactions) displayed a slow degradation in biologically mimicking conditions [48]. Based on these results, the presence of the dual crosslinking (host-guest plus electrostatic interactions) on the DOX + DOPA-rGO@$P_{CD}A_{Ca}$Gel and DOPA-rGO@$P_{CD}A_{Ca}$Gel resulted in an improved degradation

profile.

Then, the water absorption capacity of the produced hydrogels (correlates to the swelling) was evaluated in biologically mimicking conditions (Fig. 1E). The DOX + DOPA-rGO@$P_{CD}A_{Ca}$Gel and DOPA-rGO@$P_{CD}A_{Ca}$Gel demonstrated nearly identical water absorption profiles (Fig. 1E). The water uptake of these formulations peaked to 50–62 % during the first 60 min. At this initial stage, the increased osmotic pressure within the hydrogels' network could promote a high-water absorption capacity. Afterwards, the water uptake of these formulations started to decrease, reaching 37–41 % after 180 min. Such behavior may be explained by the gradual removal of the solution fraction, diminishing the osmotic pressure within the hydrogels' network and causing them to lose the previously absorbed solvent. From this timepoint onwards, DOX + DOPA-rGO@$P_{CD}A_{Ca}$Gel and DOPA-rGO@$P_{CD}A_{Ca}$Gel did not display water absorption capacity since they started to degrade/disintegrate (*e.g.*, by hydrolysis or diffusion; Fig. S8). Thus, the DOX + DOPA-rGO@$P_{CD}A_{Ca}$Gel and DOPA-rGO@$P_{CD}A_{Ca}$Gel exhibited a controlled and short-lived water uptake in biologically mimicking conditions, suggesting a well-managed swelling. Such is of utmost importance since an excessive and long-lasting swelling could jeopardize the applicability of these hydrogels by potentially causing discomfort/pain after their injection [45]. Compared to DOX + DOPA-rGO@$P_{CD}A_{Ca}$Gel and DOPA-rGO@$P_{CD}A_{Ca}$Gel, the single-crosslinked hydrogels had very different water absorption capacities.

The DOPA-rGO@P_{CD}Gel only absorbed water minimally by ≈ 2 % for 15 min (Fig. 1E). The absence of a meaningful water uptake by DOPA-rGO@P_{CD}Gel is correlated with its close-to-instantaneous degradation when immersed in biologically mimicking medium (Fig. S8). On the other hand, the DOPA-rGO@A_{Ca}Gel revealed maximum water absorption of approximately 73 % after 180 min (Fig. 1E). The water uptake of DOPA-rGO@A_{Ca}Gel remained high at 59 % even after 720 min (Fig. 1E). The long-lasting water absorption of DOPA-rGO@A_{Ca}Gel might be an impediment for its local administration. Indeed, Yu et al. also observed that composite hydrogels with a greater content of Alginate-$CaCl_2$ (electrostatic interaction) could display a swelling as high as 62 % even after 24 h [49]. Taken together, these results highlighted that the dual crosslinking (host-guest and electrostatic interactions) on the DOX + DOPA-rGO@$P_{CD}A_{Ca}$Gel and DOPA-rGO@$P_{CD}A_{Ca}$Gel led to an ameliorated water absorption capacity, suggesting a well-managed swelling profile.

Overall, the DOX + DOPA-rGO@$P_{CD}A_{Ca}$Gel and DOPA-rGO@$P_{CD}A_{Ca}$Gel exhibited an enhanced degradation and water absorption behaviours, being these formulations selected for the subsequent assays.

3.2. Assessment of the photothermal capacity of DOPA-rGO@$P_{CD}A_{Ca}$Gel and DOX + DOPA-rGO@$P_{CD}A_{Ca}$Gel and the DOX release profile

After confirming the improved physicochemical properties of DOX + DOPA-rGO@$P_{CD}A_{Ca}$Gel and DOPA-rGO@$P_{CD}A_{Ca}$Gel, the photothermal capacity of these macroscale systems was assessed (Fig. 2A). To do so, DOX + DOPA-rGO@$P_{CD}A_{Ca}$Gel and DOPA-rGO@$P_{CD}A_{Ca}$Gel (56.5 μg/mL of DOPA-rGO) were exposed to NIR light for 10 min (808 nm, 1.7 W/cm^2), being the temperature changes recorded. After 10 min of laser irradiation, the DOX + DOPA-rGO@$P_{CD}A_{Ca}$Gel and DOPA-rGO@$P_{CD}A_{Ca}$Gel produced a photoinduced heat of 13.9 and 13.7 °C (ΔT), respectively. Such hyperthermic effects can potentially damage cancer cells or sensitize them to the action of chemotherapeutics, laying the foundation for an enhanced therapeutic outcome [16,17].

As control, a dual-crosslinked hydrogel without DOPA-rGO (termed as $P_{CD}A_{Ca}$Gel) was also exposed to NIR light but, as expected, it did not generate a meaningful temperature increase (ΔT = 3.5 °C; Fig. 2A). Water (control) irradiated with NIR light also displayed a scarce temperature variation (ΔT = 2.9 °C; Fig. 2A), which is in consistent with its weak interaction with NIR radiation [17,50]. Therefore, the good photothermal capacity of DOX + DOPA-rGO@$P_{CD}A_{Ca}$Gel and DOPA-rGO@$P_{CD}A_{Ca}$Gel is related with the presence of DOPA-rGO in these formulations, which has a high NIR absorption (Fig. S1D). As anticipated, the inclusion of DOX in DOX + DOPA-rGO@$P_{CD}A_{Ca}$Gel did not impact the hydrogels' photothermal capacity since DOX does not have capacity to interact with NIR light [47,51].

Recently, Melo and colleagues produced a Chitosan-$NaHCO_3$ hydrogel incorporating DOPA-rGO (66.7 μg/mL), which produced a photoinduced heat (ΔT) of ≈12 °C upon NIR laser incidence (808 nm, 1.7 W/cm^2, 10 min) [42]. Jiang et al. prepared Poly(ethylene glycol)-based hydrogels crosslinked with Palladium nanosheets (photothermal agent), which generated a temperature increase (ΔT) of around 11 °C upon irradiation with NIR light (808 nm, 0.6 W/cm^2, 10 min) [51]. Shen team loaded ZnO-Graphene Oxide nanocomposites (photothermal agent) into a Chitosan hydrogel, verifying the capacity of this formulation to mediate a temperature increase (ΔT) of 10.2 °C upon NIR laser exposure (100 μg/mL of nanocomposites; 808 nm, 2.0 W/cm^2, 6 min) [52]. Herein, the interaction of DOX + DOPA-rGO@$P_{CD}A_{Ca}$Gel and DOPA-rGO@$P_{CD}A_{Ca}$Gel with NIR light (808 nm, 1.7 W/cm^2, 10 min) led to a temperature increase (ΔT) of 13.9 and 13.7 °C, respectively, further attesting the good photothermal capacity of these macroscale systems.

Then, the ability of the dual-crosslinked hydrogel to encapsulate DOX was studied. In this regard, the DOX + DOPA-rGO@$P_{CD}A_{Ca}$Gel exhibited a remarkable DOX encapsulation efficiency of 97 ± 2 % (n =

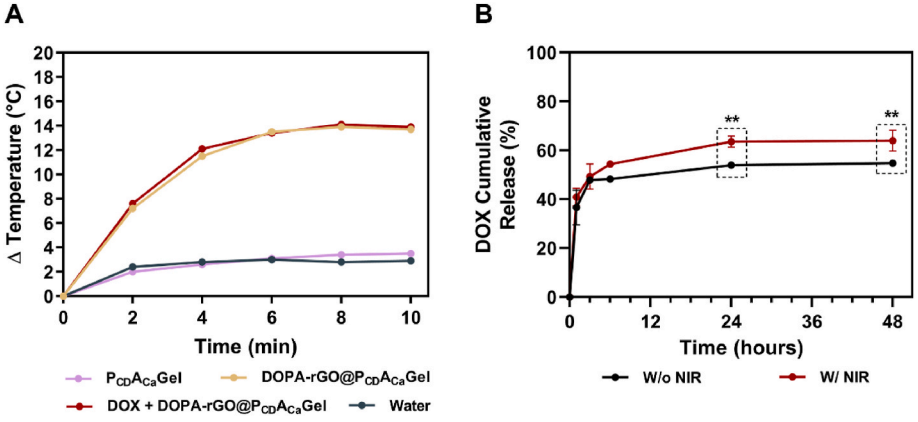

Fig. 2. Assessment of the photothermal capacity of DOPA-rGO@$P_{CD}A_{Ca}$Gel and DOX + DOPA-rGO@$P_{CD}A_{Ca}$Gel as well as the DOX release profile. (A) Temperature variation curves of DOX + DOPA-rGO@$P_{CD}A_{Ca}$Gel, DOPA-rGO@$P_{CD}A_{Ca}$Gel, $P_{CD}A_{Ca}$Gel and Water during 10 min of NIR laser irradiation (808 nm, 1.7 W/cm^2). (B) Release of DOX from DOX + DOPA-rGO@$P_{CD}A_{Ca}$Gel without (W/o NIR) and with NIR laser irradiation (W/NIR; 808 nm, 1.7 W/cm^2, 10 min). Data represents mean ± S.D., n = 3 (**$p < 0.01$).

3). Afterwards, the impact of NIR laser exposure on the release of DOX from DOX + DOPA-rGO@$P_{CD}A_{Ca}$Gel was investigated (Fig. 2B). In the absence of NIR light, the DOX + DOPA-rGO@$P_{CD}A_{Ca}$Gel released 37 % and 48 % of its DOX content within the first and third hours, respectively. After this timepoint, the amount of DOX released from DOX + DOPA-rGO@$P_{CD}A_{Ca}$Gel progressed into a plateau, being 55 % of DOX released after 48 h. Hence, the DOX + DOPA-rGO@$P_{CD}A_{Ca}$Gel displayed a burst release of DOX in the first hours, followed by a sustained release. Considering the envisioned administration route for DOX + DOPA-rGO@$P_{CD}A_{Ca}$Gel (intratumoral injection), its capacity to initially deliver locally a high drug dose may prompt a strong therapeutic outcome [53,54]. The good initial porosity of DOX + DOPA-rGO@$P_{CD}A_{Ca}$Gel may also play a role on its capacity to release DOX (Fig. S7). Moreover, the DOX + DOPA-rGO@$P_{CD}A_{Ca}$Gel ability to sustain the DOX release overtime may potentially contribute to diminish the likelihood of tumor relapse [55,56]. Such drug release profile from DOX + DOPA-rGO@$P_{CD}A_{Ca}$Gel is likely to be mainly controlled by the hydrogels' swelling (Fig. 1E), but it may also be impacted by the hydrogels' degradation kinetics (Fig. 1D and S7). Considering that a full DOX release was not achieved (*i.e.*, 100 %), interactions between the DOX and the hydrogels' polymeric network may also play a role on conditioning the drug release profile. On the other hand, when DOX + DOPA-rGO@$P_{CD}A_{Ca}$Gel was exposed to NIR light (808 nm, 1.7 W/cm^2, 10 min) at the 2-h mark, there was a slightly increase in the amount of DOX released (Fig. 2B).

In fact, the irradiation of DOX + DOPA-rGO@$P_{CD}A_{Ca}$Gel with NIR light could enhance the DOX released by up to 1.18-times (Fig. 2B). Such NIR light-augmented DOX release may result from a photothermally-induced expansion/destabilization of the hydrogels' polymeric network (Fig. S9) or from a photothermally-enhanced drug diffusion [57].

The NIR light-enhanced DOX release from DOX + DOPA-rGO@$P_{CD}A_{Ca}$Gel may open a venue for an improved chemo-photothermal effect.

3.3. Assessment of the cytocompatibility of DOPA-rGO@$P_{CD}A_{Ca}$Gel

After confirming the DOPA-rGO@$P_{CD}A_{Ca}$Gel improved physicochemical properties (injectability, *in situ* gelation, degradability and water absorption capacity) as well as its suitable photothermal capacity, the cytocompatibility of this formulation was assessed (Fig. 3A). For this purpose, NHDF (healthy cells) and MCF-7 cells (breast cancer cells) were incubated with DOPA-rGO@$P_{CD}A_{Ca}$Gel for 24 and 48 h, being then the cells' viability determined through the resazurin assay (Fig. 3B and C). The DOPA-rGO@$P_{CD}A_{Ca}$Gel demonstrated an excellent cytocompatibility profile towards both cell lines (Fig. 3B and C). In fact, NHDF incubated with DOPA-rGO@$P_{CD}A_{Ca}$Gel during 24 and 48 h displayed a viability of 90 and 92 %, respectively (Fig. 3B). Similarly, MCF-7 cells exposed to DOPA-rGO@$P_{CD}A_{Ca}$Gel for 24 and 48 h also presented a viability of 102 and 85 %, respectively (Fig. 3C).

The obtained results are aligned with good cytocompatibility of hydrogels assembled using Pluronic F127/α-Cyclodextrin and Alginate/Ca^{2+} reported elsewhere [41,58]. For example, Xu and colleagues verified that NIH 3T3 cells exposed to a Pluronic F127/α-Cyclodextrin hydrogel for 24 h remained with a viability of ≈91 % [41]. In another work, Zhang's team prepared a hydrogel based on Alginate, $CaCO_3$, and Gluconic acid lactone (the reaction between gluconic acid lactone and $CaCO_3$ yields Ca^{2+}), verifying its cytocompatibility towards 4T1 cells (viability of ≈82 % after 24 h of hydrogels' incubation) [58]. Furthermore, our research group has also demonstrated the good cytocompatibility of the DOPA-rGO as a nanomaterial and when encapsulated in hydrogels [19,42,47].

Taken together, these results further attest the DOPA-rGO@$P_{CD}A_{Ca}$Gel cytocompatibility, enabling the use of this dual-crosslinked macroscale system for phototherapeutic applications.

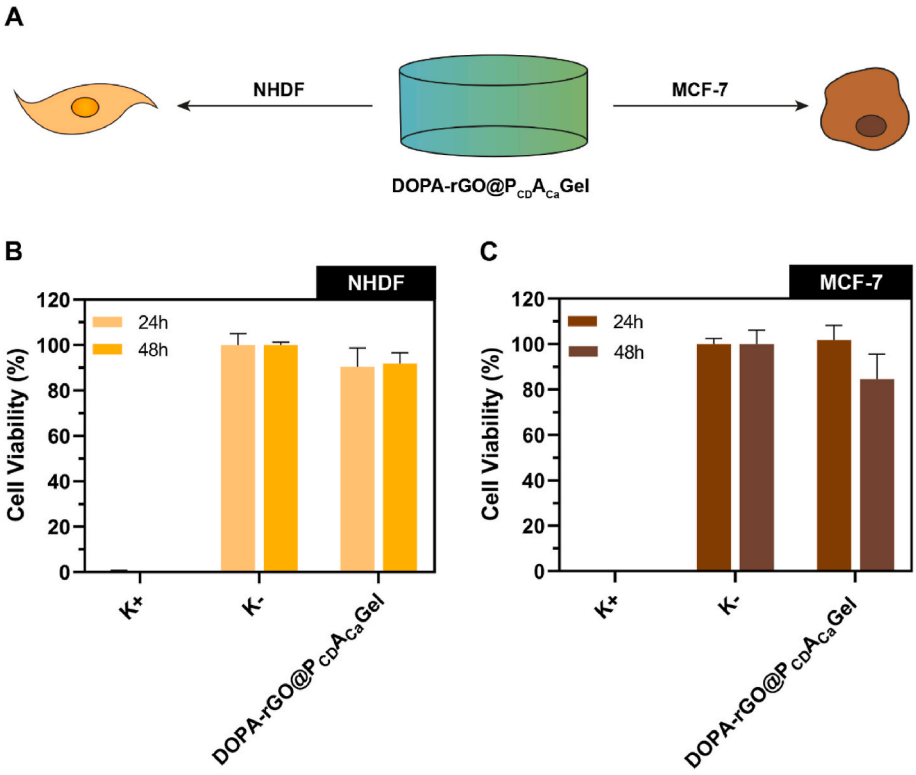

Fig. 3. Assessment of the cytocompatibility of the DOPA-rGO@$P_{CD}A_{Ca}$Gel. (A) Illustrative representation of the cytocompatibility assay. Viability of (B) NHDF and (C) MCF-7 cells incubated with DOPA-rGO@$P_{CD}A_{Ca}$Gel for 24 and 48 h (determined through the resazurin assay). Data represents mean ± S.D., n = 5. K^- and K^+ denote the negative and positive controls, respectively.

3.4. Evaluation of the photothermal therapy mediated by DOPA-rGO@$P_{CD}A_{Ca}$Gel and chemo-photothermal therapy mediated by DOX + DOPA-rGO@$P_{CD}A_{Ca}$Gel

Subsequently, the photothermal therapy mediated by DOPA-rGO@$P_{CD}A_{Ca}$Gel (56.5 μg/mL of DOPA-rGO) and chemo-photothermal therapy mediated by DOX + DOPA-rGO@$P_{CD}A_{Ca}$Gel (56.5 μg/mL of DOPA-rGO; 24.4 μg/mL of DOX) were assessed on MCF-7 cells through the resazurin assay (Fig. 4A). With this in mind, the MCF-7 cells were incubated with hydrogels, being then exposed to NIR light (808 nm, 1.7 W/cm^2, 10 min) (Fig. 4A).

As anticipated, MCF-7 cells exposed to just NIR light did not exhibit variations in their viability (≈97 %; Fig. 4B). Such result is in agreement with the scarce temperature variation obtained when water was irradiated with NIR light (ΔT < 3 °C). In fact, the NIR light *per se* has minimal interactions with biological components (*e.g.*, water, melanin, hemoglobin), and thus, it is not impactful on cells' viability [47,59,60].

Similarly, MCF-7 cells exposed to DOPA-rGO@$P_{CD}A_{Ca}$Gel also remained highly viable (≈102 %; Fig. 4B), being in agreement with the cytocompatibility results reported in the previous section (Fig. 3C). Surprisingly, the combined action of DOPA-rGO@$P_{CD}A_{Ca}$Gel and NIR light (*i.e.*, hydrogels' photothermal therapy) did not decrease meaningfully the viability of the cancer cells (≈98 %; Fig. 4B). Such data implies that the hydrogels' photothermal effect *per se* is not capable of inducing the cancer cells' death. In turn, the DOX + DOPA-rGO@$P_{CD}A_{Ca}$Gel (*i.e.*, hydrogels' chemotherapy) lowered slightly the cancer cells' viability to 70 % (Fig. 4B). Considering that the action of free DOX decreased the cancer cells' viability to ≈12 % (Fig. S10), this data highlights the ability of DOX + DOPA-rGO@$P_{CD}A_{Ca}$Gel to control the release of DOX, paving the way for an on-demand therapeutic outcome. In fact, the combined action of DOX + DOPA-rGO@$P_{CD}A_{Ca}$Gel and NIR light (*i.e.*, hydrogels' chemo-photothermal therapy) diminished the cancer cells' viability to just 23 % (Fig. 4B). Thereby, the improved outcome prompted by DOX + DOPA-rGO@$P_{CD}A_{Ca}$Gel plus NIR light may be correlated with the ability of the hydrogels' photothermal heating to boost the DOX release and to sensitize cancer cells to DOX action. In this way, the DOX + DOPA-rGO@$P_{CD}A_{Ca}$Gel had an excellent control over the therapeutic outcome since it barely affected the breast cancer cells (viability ≈ 70 %), but upon NIR laser irradiation, the efficacy of this dual-crosslinked macroscale system was boosted by ≈ 3.04-times, leading to cancer cells' ablation (viability ≈ 23 %) – Fig. 4B. This trend was also corroborated by the CellTiter-Glo® 2.0 assay (ATP-based cell viability determination; Fig. S11) and by Calcein-AM/PI staining (Live/Dead imaging; Fig. S12).

For instance, Chen et al. developed a chitosan/oxidized-konjac glucomannan injectable hydrogel containing gold nanoparticles (photothermal agent) and Oxaliplatin@cucurbit[7]uril (100 μM of Oxaliplatin; chemotherapeutic drug-loaded carrier) [61]. When irradiated two-times with NIR light for 10 min (808 nm, 2 W/cm^2), this hydrogel mediated a chemo-photothermal effect that reduced HCT116 cells' viability to 23.2 % [61]. Lima-Sousa et al. prepared a chitosan-agarose injectable hydrogel that incorporated reduced graphene oxide (10 μg/mL; photothermal nanoagent) and a DOX-Ibuprofen combination (90.4 μM; chemotherapeutic cocktail), which after exposure to NIR light (808 nm, 1.7 W/cm^2, 10 min), reduced the viability of MCF-7 cells to 34 % [45]. In this work, the combination of DOX + DOPA-rGO@$P_{CD}A_{Ca}$Gel (56.5 μg/mL of DOPA-rGO; 24.4 μg/mL of DOX) with NIR laser irradiation (808 nm, 1.7 W/cm^2, 10 min) diminished the viability of breast cancer cells to just 23 %. In this way, the DOX + DOPA-rGO@$P_{CD}A_{Ca}$Gel is a promising dual-crosslinked macroscale system for application in the chemo-photothermal therapy of breast cancer cells.

4. Conclusion

In this work, a dual-crosslinked injectable *in situ* forming hydrogel was engineered by combining Pluronic F127/α-Cyclodextrin and Alginate/$CaCl_2$ (host-guest plus electrostatic interactions), being loaded with DOX and DOPA-rGO to be applied, for the first time, in cancer chemo-photothermal therapy. The dual-crosslinked hydrogels (DOX + DOPA-rGO@$P_{CD}A_{Ca}$Gel and DOPA-rGO@$P_{CD}A_{Ca}$Gel) showed injectability and *in situ* gelation capacity as well as suitable degradation and water absorption capacity behaviors. In contrast, the single-crosslinked hydrogels had a very different behavior. Even though the DOPA-rGO@P_{CD}Gel (host-guest crosslinked hydrogel) displayed injectability and *in situ* gelation, this formulation had a premature degradation in biologically mimicking medium. In turn, the DOPA-rGO@A_{Ca}Gel (electrostatic crosslinked hydrogel) did not present injectability, had an irregular incorporation of the therapeutics, and displayed a long-lasting water uptake. Therefore, the dual-crosslinking (host-guest plus electrostatic interactions) present on DOX + DOPA-rGO@$P_{CD}A_{Ca}$Gel and

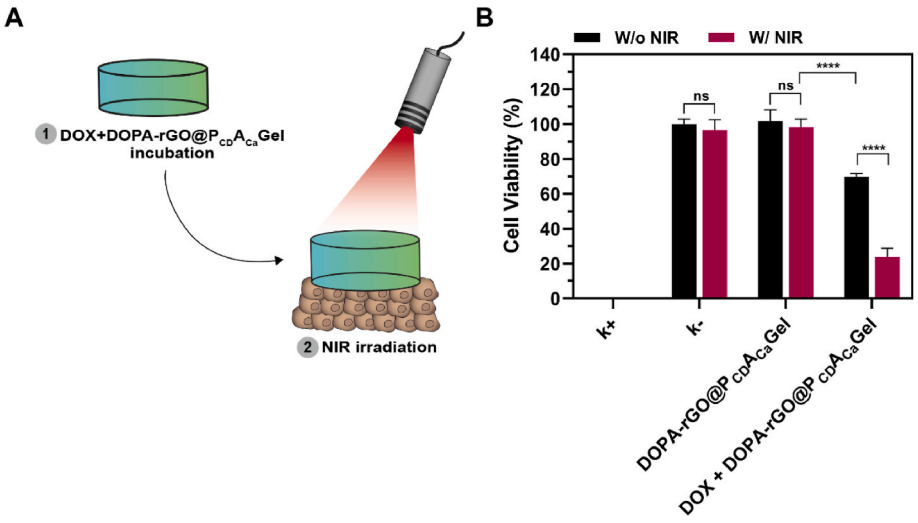

Fig. 4. Evaluation of the photothermal therapy mediated by DOPA-rGO@$P_{CD}A_{Ca}$Gel and chemo-photothermal therapy mediated by DOX + DOPA-rGO@$P_{CD}A_{Ca}$Gel. (A) Schematic illustration of the chemo-photothermal therapy mediated by DOX + DOPA-rGO@$P_{CD}A_{Ca}$Gel. (B) Viability of MCF-7 cells exposed to DOPA-rGO@$P_{CD}A_{Ca}$Gel (56.5 μg/mL of DOPA-rGO) and DOX + DOPA-rGO@$P_{CD}A_{Ca}$Gel (56.5 μg/mL of DOPA-rGO; 24.4 μg/mL of DOX) without (W/o NIR) and with NIR laser irradiation (W/NIR; 808 nm, 1.7 W/cm^2, 10 min) (assessed by the resazurin assay). Data represents mean ± S.D., n = 5 (****$p < 0.0001$, ns = non-significant). K^- W/o NIR represents the negative control (*i.e.*, non-treated cells). K^- W/NIR corresponds to cells only exposed to NIR light. K^+ W/o NIR denotes the positive control (*i.e.*, ethanol treated cells). K^+ W/NIR denotes ethanol treated cells exposed to NIR light.

DOPA-rGO@$P_{CD}A_{Ca}$Gel contributed to the assembly of formulations with improved physicochemical properties. Moreover, the DOX + DOPA-rGO@$P_{CD}A_{Ca}$Gel and DOPA-rGO@$P_{CD}A_{Ca}$Gel displayed a good photothermal capacity, being able to mediate a temperature increase of ≈14 °C (ΔT) upon NIR laser irradiation. Such photothermal heating also improved the release of DOX from DOX + DOPA-rGO@$P_{CD}A_{Ca}$Gel by 1.18 times. The *in vitro* studies highlighted the good cytocompatibility of DOPA-rGO@$P_{CD}A_{Ca}$Gel towards both NHDF and MCF-7 cells. When MCF-7 cells were exposed to DOPA-rGO@$P_{CD}A_{Ca}$Gel plus NIR light (hydrogels' photothermal therapy), their viability remained at 98 %. In turn, DOX + DOPA-rGO@$P_{CD}A_{Ca}$Gel (hydrogels' chemotherapy) only decreased the cancer cells' viability to 70 %. In stark contrast, the combined action of DOX + DOPA-rGO@$P_{CD}A_{Ca}$Gel and NIR light (hydrogels' chemo-photothermal therapy) diminished the cancer cells' viability to just 23 %. Overall, the DOX + DOPA-rGO@$P_{CD}A_{Ca}$Gel is a promising macroscale system for the chemo-photothermal therapy of breast cancer cells. In the future, *in vivo* studies will be crucial to validate the hydrogels' biodegradability, biocompatibility and chemo-photothermal capacity on more complex models. Moreover, the hydrogels' chemo-photothermal capacity may also be explored in the treatment of other cancers (*e.g.*, melanoma). Additional agents (*e.g.*, photosensitizers, immunomodulators) can also be encapsulated in these dual-crosslinked hydrogels to unlock other combinatorial therapeutic modalities.

CRediT authorship contribution statement

Joaquim J. Gonçalves: Writing – original draft, Investigation, Formal analysis, Conceptualization. **Bruna L. Melo:** Writing – review & editing, Investigation. **Manuel R. Pouso:** Writing – review & editing, Investigation. **Ilídio J. Correia:** Writing – review & editing, Supervision, Project administration, Funding acquisition. **Duarte de Melo-Diogo:** Writing – review & editing, Supervision, Project administration, Funding acquisition, Conceptualization.

Declaration of competing interest

The authors declare that they have no known competing financial interests or personal relationships that could have appeared to influence the work reported in this paper.

Acknowledgments

This research was funded in whole or in part by the Fundação para a Ciência e a Tecnologia, I.P. (FCT, https://ror.org/00snfqn58) under the Grants 10.54499/UIDB/00709/2020 (https://doi.org/10.54499/UIDB/00709/2020), 10.54499/UIDP/00709/2020 (https://doi.org/10.54499/UIDP/00709/2020), PTDC/BTABTA/0696/2020, 2022.06320.PTDC (DOI 10.54499/2022.06320.PTDC), 10.54499/LA/P/0079/2020 and 10.54499/UIDB/50022/2020. The project COMPETE2030-FEDER-00695800 is also acknowledged. Duarte de Melo-Diogo acknowledges FCT for the financial support given through a Junior Researcher contract (2021.00590.CEECIND; DOI 10.54499/2021.00590.CEECIND/CP1661/CT0001). Manuel R. Pouso acknowledges a Research Fellowship funded by the project 2022.06320.PTDC (DOI 10.54499/2022.06320.PTDC). The funding from individual PhD fellowships from FCT is acknwoledged by Bruna L. Melo (2021.06044.BD; https://doi.org/10.54499/2021.06044.BD) and Manuel R. Pouso (2024.01490.BD). The authors thank the technical support of the Fluorescence Microscopy Unit of RISE-Health, UBI, integrated in the national infrastructure PPBI - Portuguese Platform of Bioimaging. For the purpose of Open Access, the authors have applied a CC-BY public copyright license to any Author's Accepted Manuscript (AAM) version arising from this submission.

Appendix A. Supplementary data

Supplementary data to this article can be found online at https://doi.org/10.1016/j.jddst.2025.107520.

Data availability

Data will be made available on request.

References

[1] A.C. Anselmo, S. Mitragotri, Nanoparticles in the clinic: an update post COVID-19 vaccines, Bioeng. Translat. Med. 6 (2021) e10246.
[2] R. Liu, C. Luo, Z. Pang, J. Zhang, S. Ruan, M. Wu, L. Wang, T. Sun, N. Li, L. Han, J. Shi, Y. Huang, W. Guo, S. Peng, W. Zhou, H. Gao, Advances of nanoparticles as drug delivery systems for disease diagnosis and treatment, Chin. Chem. Lett. 34 (2023) 107518.
[3] M.J. Mitchell, M.M. Billingsley, R.M. Haley, M.E. Wechsler, N.A. Peppas, R. Langer, Engineering precision nanoparticles for drug delivery, Nat. Rev. Drug Discov. 20 (2021) 101–124.
[4] M. Ikeda-Imafuku, L.L.-W. Wang, D. Rodrigues, S. Shaha, Z. Zhao, S. Mitragotri, Strategies to improve the EPR effect: a mechanistic perspective and clinical translation, J. Contr. Release 345 (2022) 512–536.
[5] P. Makvandi, M. Ghomi, M. Ashrafizadeh, A. Tafazoli, T. Agarwal, M. Delfi, J. Akhtari, E.N. Zare, V.V. Padil, A. Zarrabi, A review on advances in graphene-derivative/polysaccharide bionanocomposites: therapeutics, pharmacogenomics and toxicity, Carbohydr. Polym. 250 (2020) 116952.
[6] H. Cabral, J. Li, K. Miyata, K. Kataoka, Controlling the biodistribution and clearance of nanomedicines, Nat. Rev. Bioeng. 2 (2024) 214–232.
[7] M.J. Ernsting, M. Murakami, A. Roy, S.-D. Li, Factors controlling the pharmacokinetics, biodistribution and intratumoral penetration of nanoparticles, J. Contr. Release 172 (2013) 782–794.
[8] B. Shrestha, L. Tang, G. Romero, Nanoparticles-mediated combination therapies for cancer treatment, Adv. Therapeut. 2 (2019) 1900076.
[9] H. Wang, Y. Huang, Combination therapy based on nano codelivery for overcoming cancer drug resistance, Med. Drug Discov. 6 (2020) 100024.
[10] J. Wang, X. Wu, P. Shen, J. Wang, Y. Shen, Y. Shen, T.J. Webster, J. Deng, Applications of inorganic nanomaterials in photothermal therapy based on combinational cancer treatment, Int. J. Nanomed. (2020) 1903–1914.
[11] X. Cui, Q. Ruan, X. Zhuo, X. Xia, J. Hu, R. Fu, Y. Li, J. Wang, H. Xu, Photothermal nanomaterials: a powerful light-to-heat converter, Chem. Rev. 123 (2023) 6891–6952.
[12] Z. Li, Y. Chen, Y. Yang, Y. Yu, Y. Zhang, D. Zhu, X. Yu, X. Ouyang, Z. Xie, Y. Zhao, Recent advances in nanomaterials-based chemo-photothermal combination therapy for improving cancer treatment, Front. Bioeng. Biotechnol. 7 (2019) 293.
[13] V. Patel, C. Rajani, V. Tambe, D. Kalyane, N. Anup, P.K. Deb, K. Kalia, R.K. Tekade, Nanomaterials assisted chemo-photothermal therapy for combating cancer drug resistance, J. Drug Deliv. Sci. Technol. 70 (2022) 103164.
[14] J. Li, Z. Lyv, Y. Li, H. Liu, J. Wang, W. Zhan, H. Chen, H. Chen, X. Li, A theranostic prodrug delivery system based on Pt (IV) conjugated nano-graphene oxide with synergistic effect to enhance the therapeutic efficacy of Pt drug, Biomaterials 51 (2015) 12–21.
[15] Y. Long, X. Wu, Z. Li, J. Fan, X. Hu, B. Liu, PEGylated WS 2 nanodrug system with erythrocyte membrane coating for chemo/photothermal therapy of cervical cancer, Biomater. Sci. 8 (2020) 5088–5105.
[16] J. Chen, C. Ning, Z. Zhou, P. Yu, Y. Zhu, G. Tan, C. Mao, Nanomaterials as photothermal therapeutic agents, Prog. Mater. Sci. 99 (2019) 1–26.
[17] R. Lima-Sousa, C.G. Alves, B.L. Melo, F.J. Costa, M. Nave, A.F. Moreira, A. G. Mendonça, I.J. Correia, D. de Melo-Diogo, Injectable hydrogels for the delivery of nanomaterials for cancer combinatorial photothermal therapy, Biomater. Sci. 11 (2023) 6082–6108.
[18] X. Wang, Z. Xuan, X. Zhu, H. Sun, J. Li, Z. Xie, Near-infrared photoresponsive drug delivery nanosystems for cancer photo-chemotherapy, J. Nanobiotechnol. 18 (2020) 108.
[19] R. Lima-Sousa, C.G. Alves, B.L. Melo, A.F. Moreira, A.G. Mendonca, I.J. Correia, D. de Melo-Diogo, Poly (2-ethyl-2-oxazoline) functionalized reduced graphene oxide: optimization of the reduction process using dopamine and application in cancer photothermal therapy, Mater. Sci. Eng. C 130 (2021) 112468.
[20] D. de Melo-Diogo, R. Lima-Sousa, C.G. Alves, I.J. Correia, Graphene family nanomaterials for application in cancer combination photothermal therapy, Biomater. Sci. 7 (2019) 3534–3551.
[21] R. Lima-Sousa, B.L. Melo, A.G. Mendonça, I.J. Correia, D. de Melo-Diogo, Hyaluronic acid-functionalized graphene-based nanohybrids for targeted breast cancer chemo-photothermal therapy, Int. J. Pharm. 651 (2024) 123763.
[22] B.L. Melo, R. Lima-Sousa, C.G. Alves, I.J. Correia, D. de Melo-Diogo, Sulfobetaine methacrylate-coated reduced graphene oxide-IR780 hybrid nanosystems for effective cancer photothermal-photodynamic therapy, Int. J. Pharm. 647 (2023) 123552.
[23] S. Wilhelm, A.J. Tavares, Q. Dai, S. Ohta, J. Audet, H.F. Dvorak, W.C. Chan, Analysis of nanoparticle delivery to tumours, Nat. Rev. Mater. 1 (2016) 1–12.
[24] Z. Fan, P. Zhu, Y. Zhu, K. Wu, C.Y. Li, H. Cheng, Engineering long-circulating nanomaterial delivery systems, Curr. Opin. Biotechnol. 66 (2020) 131–139.

[25] T.U. Wani, S.N. Raza, N.A. Khan, Nanoparticle opsonization: forces involved and protection by long chain polymers, Polym. Bull. 77 (2020) 3865–3889.
[26] A. Dhaliwal, G. Zheng, Improving accessibility of EPR-insensitive tumor phenotypes using EPR-adaptive strategies: designing a new perspective in nanomedicine delivery, Theranostics 9 (2019) 8091.
[27] L.N. Nguyen, W. Ngo, Z.P. Lin, S. Sindhwani, P. MacMillan, S.M. Mladjenovic, W. C. Chan, The mechanisms of nanoparticle delivery to solid tumours, Nat. Rev. Bioeng. 2 (2024) 201–213.
[28] D. Sun, S. Zhou, W. Gao, What went wrong with anticancer nanomedicine design and how to make it right, ACS Nano 14 (2020) 12281–12290.
[29] M.R. Pouso, B.L. Melo, J.J. Gonçalves, R.O. Louro, A.G. Mendonça, I.J. Correia, D. de Melo-Diogo, Injectable and implantable hydrogels for localized delivery of drugs and nanomaterials for cancer chemotherapy: a review, Int. J. Pharm. 677 (2025) 125640.
[30] Y.I. Cho, S. Park, S.Y. Jeong, H.S. Yoo, In vivo and in vitro anti-cancer activity of thermo-sensitive and photo-crosslinkable doxorubicin hydrogels composed of chitosan–doxorubicin conjugates, Eur. J. Pharm. Biopharm. 73 (2009) 59–65.
[31] H. Hyun, M.H. Park, W. Lim, S.Y. Kim, D. Jo, J.S. Jung, G. Jo, S. Um, D.-W. Lee, D. H. Yang, Injectable visible light-cured glycol chitosan hydrogels with controlled release of anticancer drugs for local cancer therapy in vivo: a feasible study, Artif. Cell Nanomed. Biotechnol. 46 (2018) 874–882.
[32] Y.-J. Jo, M. Gulfam, S.-H. Jo, Y.-S. Gal, C.-W. Oh, S.-H. Park, K.T. Lim, Multi-stimuli responsive hydrogels derived from hyaluronic acid for cancer therapy application, Carbohydr. Polym. 286 (2022) 119303.
[33] Y.-W. Lo, M.-T. Sheu, W.-H. Chiang, Y.-L. Chiu, C.-M. Tu, W.-Y. Wang, M.-H. Wu, Y.-C. Wang, M. Lu, H.-O. Ho, In situ chemically crosslinked injectable hydrogels for the subcutaneous delivery of trastuzumab to treat breast cancer, Acta Biomater. 86 (2019) 280–290.
[34] A. Rizwan, M. Gulfam, S.-H. Jo, J.-W. Seo, I. Ali, T.T. Vu, S.-B. Joo, S.-H. Park, K. T. Lim, Gelatin-based NIR and reduction-responsive injectable hydrogels cross-linked through IEDDA click chemistry for drug delivery application, Eur. Polym. J. 191 (2023) 112019.
[35] H. Sadeghi-Abandansari, S. Pakian, M.-R. Nabid, M. Ebrahimi, A. Rezalotfi, Local co-delivery of 5-fluorouracil and curcumin using Schiff's base cross-linked injectable hydrogels for colorectal cancer combination therapy, Eur. Polym. J. 157 (2021) 110646.
[36] L.E. Jansen, L.J. Negrón-Piñeiro, S. Galarza, S.R. Peyton, Control of thiol-maleimide reaction kinetics in PEG hydrogel networks, Acta Biomater. 70 (2018) 120–128.
[37] M.F. Akhtar, M. Hanif, N.M. Ranjha, Methods of synthesis of hydrogels… A review, Saudi Pharm. J. 24 (2016) 554–559.
[38] J. Yang, Y. Chen, L. Zhao, J. Zhang, H. Luo, Constructions and properties of physically cross-linked hydrogels based on natural polymers, Polym. Rev. 63 (2023) 574–612.
[39] Y. Chao, L. Xu, C. Liang, L. Feng, J. Xu, Z. Dong, L. Tian, X. Yi, K. Yang, Z. Liu, Combined local immunostimulatory radioisotope therapy and systemic immune checkpoint blockade imparts potent antitumour responses, Nat. Biomed. Eng. 2 (2018) 611–621.
[40] C. Pradal, L. Grøndahl, J.J. Cooper-White, Hydrolytically degradable polyrotaxane hydrogels for drug and cell delivery applications, Biomacromolecules 16 (2015) 389–403.
[41] J. Xu, K. Wang, Y. Li, Y. Li, B. Li, H. Luo, H. Shi, X. Guan, T. Zhang, Y. Sun, Injectable host-guest supramolecular hydrogel Co-Delivers hydrophobic and hydrophilic agents for enhanced wound healing, Chem. Eng. J. 454 (2023) 140027.
[42] B.L. Melo, R. Lima-Sousa, C.G. Alves, A.F. Moreira, I.J. Correia, D. de Melo-Diogo, Chitosan-based injectable in situ forming hydrogels containing dopamine-reduced graphene oxide and resveratrol for breast cancer chemo-photothermal therapy, Biochem. Eng. J. 185 (2022) 108529.
[43] M.R. Pouso, B.L. Melo, J.J. Gonçalves, A.G. Mendonça, I.J. Correia, D. de Melo-Diogo, Development of dual-crosslinked Pluronic F127/Chitosan injectable hydrogels incorporating graphene nanosystems for breast cancer photothermal therapy and antibacterial applications, Eur. J. Pharm. Biopharm. 203 (2024) 114476.
[44] S. Simões, F. Veiga, J. Torres-Labandeira, A. Ribeiro, M. Sandez-Macho, A. Concheiro, C. Alvarez-Lorenzo, Syringeable Pluronic–α-cyclodextrin supramolecular gels for sustained delivery of vancomycin, Eur. J. Pharm. Biopharm. 80 (2012) 103–112.
[45] R. Lima-Sousa, D. de Melo-Diogo, C.G. Alves, C.S. Cabral, S.P. Miguel, A. G. Mendonça, I.J. Correia, Injectable in situ forming thermo-responsive graphene based hydrogels for cancer chemo-photothermal therapy and NIR light-enhanced antibacterial applications, Mater. Sci. Eng. C 117 (2020) 111294.
[46] K. Salma-Ancane, A. Sceglovs, E. Tracuma, J.K. Wychowaniec, K. Aunina, A. Ramata-Stunda, V. Nikolajeva, D. Loca, Effect of crosslinking strategy on the biological, antibacterial and physicochemical performance of hyaluronic acid and ε-polylysine based hydrogels, Int. J. Biol. Macromol. 208 (2022) 995–1008.
[47] F.J. Costa, M. Nave, R. Lima-Sousa, C.G. Alves, B.L. Melo, I.J. Correia, D. de Melo-Diogo, Development of Thiol-Maleimide hydrogels incorporating graphene-based nanomaterials for cancer chemo-photothermal therapy, Int. J. Pharm. 635 (2023) 122713.
[48] J. Su, H. Xu, J. Sun, X. Gong, H. Zhao, Dual delivery of BMP-2 and bFGF from a new nano-composite scaffold, loaded with vascular stents for large-size mandibular defect regeneration, Int. J. Mol. Sci. 14 (2013) 12714–12728.
[49] F. Yu, T. Cui, C. Yang, X. Dai, J. Ma, κ-Carrageenan/Sodium alginate double-network hydrogel with enhanced mechanical properties, anti-swelling, and adsorption capacity, Chemosphere 237 (2019) 124417.
[50] A.V.P. Kumar, S.K. Dubey, S. Tiwari, A. Puri, S. Hejmady, B. Gorain, P. Kesharwani, Recent advances in nanoparticles mediated photothermal therapy induced tumor regression, Int. J. Pharm. 606 (2021) 120848.
[51] Y.-W. Jiang, G. Gao, P. Hu, J.-B. Liu, Y. Guo, X. Zhang, X.-W. Yu, F.-G. Wu, X. Lu, Palladium nanosheet-knotted injectable hydrogels formed via palladium–sulfur bonding for synergistic chemo-photothermal therapy, Nanoscale 12 (2020) 210–219.
[52] Y. Liang, M. Wang, Z. Zhang, G. Ren, Y. Liu, S. Wu, J. Shen, Facile synthesis of ZnO QDs@ GO-CS hydrogel for synergetic antibacterial applications and enhanced wound healing, Chem. Eng. J. 378 (2019) 122043.
[53] D.Y. Kwon, J.S. Kwon, J.H. Park, S.H. Park, H.J. Oh, J.H. Kim, B.H. Min, K. Park, M.S. Kim, Synergistic anti-tumor activity through combinational intratumoral injection of an in-situ injectable drug depot, Biomaterials 85 (2016) 232–245.
[54] J. Liu, C. Qi, K. Tao, J. Zhang, J. Zhang, L. Xu, X. Jiang, Y. Zhang, L. Huang, Q. Li, Sericin/dextran injectable hydrogel as an optically trackable drug delivery system for malignant melanoma treatment, ACS Appl. Mater. Interfaces 8 (2016) 6411–6422.
[55] J. Xiong, J. Yan, C. Li, X. Wang, L. Wang, D. Pan, Y. Xu, F. Wang, X. Li, Q. Wu, Injectable liquid metal nanoflake hydrogel as a local therapeutic for enhanced postsurgical suppression of tumor recurrence, Chem. Eng. J. 416 (2021) 129092.
[56] Q. Zhang, Y. Zhang, H. Chen, L.-N. Sun, B. Zhang, D.-S. Yue, C.-L. Wang, Z.-F. Zhang, Injectable hydrogel with doxorubicin-loaded ZIF-8 nanoparticles for tumor postoperative treatments and wound repair, Sci. Rep. 14 (2024) 9983.
[57] C. Niu, X. Liu, Y. Wang, X. Li, J. Shi, Photothermal-modulated drug release from a composite hydrogel based on silk fibroin and sodium alginate, Eur. Polym. J. 146 (2021) 110267.
[58] Y. Zhang, T. Wang, Y. Zhuang, T. He, X. Wu, L. Su, J. Kang, J. Chang, H. Wang, Sodium alginate hydrogel-mediated cancer immunotherapy for postoperative in situ recurrence and metastasis, ACS Biomater. Sci. Eng. 7 (2021) 5717–5726.
[59] T. Dube, U.B. Kompella, J.J. Panda, Near infrared triggered chemo-PTT-PDT effect mediated by glioma directed twin functional-chimeric peptide-decorated gold nanoroses, J. Photochem. Photobiol. B Biol. 228 (2022) 112407.
[60] J. Wang, J. Han, C. Zhu, N. Han, J. Xi, L. Fan, R. Guo, Gold nanorods/polypyrrole/m-SiO2 core/shell hybrids as drug nanocarriers for efficient chemo-photothermal therapy, Langmuir 34 (2018) 14661–14669.
[61] J. Chen, H. Gu, S. Fu, J. Lu, H. Tan, Q. Wei, H. Ai, Multifunctional injectable hydrogels for three-in-one cancer therapy: preoperative remission via mild photothermal-enhanced supramolecular chemotherapy and prevention of postoperative recurrence and adhesion, Chem. Eng. J. 425 (2021) 130377.